Arch Appl Mech (2012) 82:479–494
DOI 10.1007/s00419-011-0568-2

ORIGINAL

T.-L. Zhu

Free flapewise vibration analysis of rotating double-tapered Timoshenko beams

Received: 25 July 2010 / Accepted: 7 July 2011 / Published online: 17 September 2011

Abstract Free vibration analysis of a rotating double-tapered Timoshenko beam undergoing flapwise transverse vibration is presented. Using an assumed mode method, the governing equations of motion are derived from the kinetic and potential energy expressions which are derived from a set of hybrid deformation variables. These equations of motion are then transformed into dimensionless forms using a set of dimensionless parameters, such as the hub radius ratio, the dimensionless angular speed ratio, the slenderness ratio, and the height and width taper ratios, etc. The natural frequencies and mode shapes are then determined from these dimensionless equations of motion. The effects of the dimensionless parameters on the natural frequencies and modal characteristics of a rotating double-tapered Timoshenko beam are numerically studied through numerical examples. The tuned angular speed of the rotating double-tapered Timoshenko beam is then investigated.

Keywords Free vibration · Modal characteristics · Double-tapered rotating Timoshenko beams · Hybrid deformation variables · Dimensionless parameters

1 Introduction

The modal characteristics, i.e., the natural frequencies and the corresponding mode shapes, of rotating beams, especially tapered ones, are critical to the design and analysis of rotating structures, such as the rotating machinery, helicopter blades, wind turbine blades, etc., since most rotating beams in engineering applications are tapered. The modal characteristics of rotating beams often vary significantly from those of non-rotating beams due to the influence of centrifugal inertia force. Due to this significant variation of modal characteristics resulted from rotation, the modal characteristic of rotating beams has been widely investigated.

Study of the modal characteristics of rotating beams originated from the pioneering work of Southwell and Gough [1]. Based on the Rayleigh energy theorem, an equation, known as the Southwell equation, that relates the natural frequency to the rotating frequency of a uniform beam was developed. This study was further extended by Liebers [2], Theodorsen [3] and Schilhansl [4], to obtain more accurate natural frequencies of rotating beams. However, due to the large amount of calculation and lack of computational devices, the mode shapes were not available in these investigations. Later, using digital computers, investigations in mode shapes and more accurate natural frequencies were published for uniform rotating and non-rotating beams [5–13].

The modal characteristics of rotating and non-rotating tapered beams have also been widely investigated. Hodges and Dowell [14] derived the non-linear equations of motion of twisted non-uniform rotor blades based on the Hamilton's Principle and the Newtonian method. Klein [15] analyzed the vibration of a non-rotating tapered beam with a method which combined the advantages of a finite element approach and of a Rayleigh–Ritz analysis. Downs [16] applied a dynamic discretization technique to calculate the natural frequencies of a

T.-L. Zhu (✉)
Department of Mechanical Engineering, Widener University, One University Place, Chester, PA 19013, USA
E-mail: tzhu@mail.widener.edu
Tel.: +1-610-4994061
Fax: +1-610-4994059

non-rotating double-tapered beam. Swaminathan and Rao [17] used the Ritz method to calculate the flexural frequencies of a pretwist rotating blade with a width taper. Gupta and Rao [18] applied an finite element analysis to evaluate the natural frequencies of non-rotating tapered and twisted Timoshenko beams. Hodges [19] used the direct analytical method of Ritz to solve for the modal characteristics of a non-uniform rotating beam with discontinuities. Sato [20] used the Ritz method to study the transverse vibration of a linearly tapered beam with ends constrained elastically against rotation and subjected to an axial force. Subrahmanyama and Rao [21] determined the natural frequencies and mode shapes of a pretwisted tapered blading using the Reissner method. Lau [22] studied the free vibrations of a tapered beam with an end mass using the exact method. Banerjee and his coworkers [23–25] investigated the vibration of different types of beams using the finite element method. Grossi et al [26–28] used, respectively, the Rayleigh–Ritz method and the Rayleigh–Schmidt method to analyze the truncated tapered beams with rotational constraints at both ends. Bazoune and Khulief [29] developed a finite beam element for vibration analysis of a rotating double-tapered Timoshenko beam. This work was further extended to account for different boundary conditions [30]. Naguleswaran [31–33] used the Frobenius method to analyze the free vibration of different types of non-uniform beams. Lee and Kuo [34] provided an exact solution based on the Green's function method for the dynamic analysis of a general elastically end restrained Bernoulli–Euler beam with polynomial varying bending rigidity, applied axial end force, and elastic foundation modulus along the beam, subjected to an arbitrary transverse force. Lee and Lin [35] investigated the influence of taper ratio, elastic root restraint, setting angle, and rotational speed on the bending natural frequencies of a rotating non-uniform beam using a semi-exact numerical method. This work was further extended for a Timoshenko beam [36] and to account for the effect of a tip mass [37]. Using the differential transform method in [38], Ozdemir and Kaya [39] investigated flexural vibration of a rotating double-tapered Euler–Bernoulli beam, the flapwise bending vibration of a rotating tapered cantilevered Bernoulli–Euler beam [40], and the flapwise bending vibration of a rotating double-tapered Timoshenko beam [41].

In the present study, free vibration of a rotating, double-tapered, cantilever Timoshenko beam that undergoes flapwise transverse vibration is investigated using the hybrid deformation variables introduced in Kane et al. [42] and in Yoo et al [11,43,44]. The combined effect of angular speed, hub radius, slenderness ratio, shear/extension modulus ratio, and the height and width taper ratios on the modal characteristics of a rotating Timoshenko beam is successfully investigated in this study. The tuned angular speed, which does not exist in the rotating Euler–Bernoulli beam undergoing flapwise bending vibration, is also found for a uniform rotating Timoshenko beam.

2 Equations of motion

2.1 Approximation of deformation variables

The governing equations of motion are derived for the flapwise transverse vibration of a rotating double-tapered Timoshenko beam shown in Fig. 1. The following assumptions are made in the present work so as to simplify the formulations and to focus on the critical effects due to rotation.

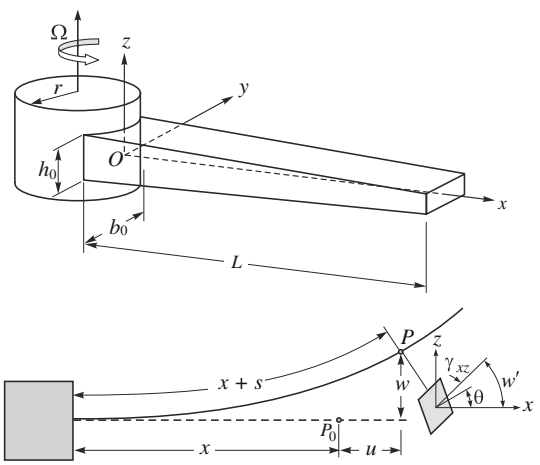

Fig. 1 Configuration of the beam and the deformation of the beam and the neutral axis

– The flapwise transverse displacement is small.
– The neutral and centroidal axes in the cross-section of the beam coincide so that neither eccentricity nor torsion needs to be considered.
– The planar cross-sections that are initially perpendicular to the neutral axis of the beam remain plane, but no longer perpendicular to the neutral axis.
– The material of the Timoshenko beam is homogeneous and isotropic.

Figure 1 also shows the deformation of the beam and the deformation of the neutral axis of the beam. A generic point P_0 which lies on the undeformed neutral axis moves to P when the beam is deformed. Two Cartesian variables u and w are shown to describe the deformation of point P in the x- and z-directions, respectively. θ is the rotational angle of the cross-section in the x–z plane. The stretch of the arc length of the neutral axis, s, is also shown in Fig. 1. The arc length stretch, s, a non-Cartesian variable will be used, instead of u, to compute the strain and kinetic energies. The strains and rotational angles at each cross-section of the beam are also shown in the figure.

In the present study, the arc length stretch s will be used in deriving the equations of motion. To do this, the geometric relation between the arc length stretch s and the Cartesian variables is required. This relation is given in Ref. [45], as

$$u = s - \frac{1}{2}\int_0^x \left(w'\right)^2 d\sigma \tag{1}$$

where a symbol with a prime ($'$) represents the partial derivative with respect to the integral domain variable.

In the present work, s, w, and θ are approximated by spatial functions and the corresponding coordinates. By employing the Rayleigh–Ritz method, the deformation variables are approximated as follows [11]

$$s(x,t) = \sum_{j=1}^{\mu_1} \phi_{1j}(x) q_{1j}(t) \tag{2}$$

$$w(x,t) = \sum_{j=1}^{\mu_2} \phi_{2j}(x) q_{2j}(t) \tag{3}$$

$$\theta(x,t) = \sum_{j=1}^{\mu_3} \phi_{3j}(x) q_{3j}(t) \tag{4}$$

In the above equations, ϕ_{1j}, ϕ_{2j}, and ϕ_{3j} are the assumed modal functions for s, w, and θ, respectively. The q_{ij}'s are the generalized coordinates, and μ_1, μ_2, and μ_3 are the number of assumed modes used for s, w, and θ, respectively. The total number of modes, μ, equals the summation of these individual number of modes, i.e.,

$$\mu = \mu_1 + \mu_2 + \mu_3 \tag{5}$$

2.2 The strain energy of the system

The potential energy of a Timoshenko beam, employing the hybrid set of deformation variables, is given by [46]

$$U = \frac{1}{2}\int_0^L \left[EA\left(\frac{\partial s}{\partial x}\right)^2 + EI\left(\frac{\partial \theta}{\partial x}\right)^2 + kAG\left(\theta - \frac{\partial w}{\partial x}\right)^2 \right] dx \tag{6}$$

where E is the Young's modulus, G is the shear modulus, k is the shear correction factor, A is the cross-sectional area, I is the second area moment of inertia of the cross-section about the y-axis , and L is the length of the beam.

Substituting Eqs. (2)–(4) into Eq. (6), one obtains the following potential energy expression in terms of the generalized coordinates, q_{ij}

$$U = \frac{1}{2}\int_0^L \left[EA\left(\sum_{j=1}^{\mu_1}\phi'_{1j}q_{1j}\right)^2 + EI\left(\sum_{j=1}^{\mu_3}\phi'_{3j}q_{3j}\right)^2 + kAG\left(\sum_{j=1}^{\mu_3}\phi_{3j}q_{3j} - \sum_{j=1}^{\mu_2}\phi'_{2j}q_{2j}\right)^2\right] \mathrm{d}x \tag{7}$$

To derive the equations of motion of the rotating beam, the partial derivatives of U with respect to the generalized coordinates, q_{ij}, are required. Differentiating U partially with respect to q_{1i}, q_{2i}, and q_{3i}, respectively, in Eq. (7) yields

$$\frac{\partial U}{\partial q_{1i}} = \int_0^L EA\sum_{j=1}^{\mu_1}\phi'_{1i}\phi'_{1j}q_{1j}\mathrm{d}x \tag{8}$$

$$\frac{\partial U}{\partial q_{2i}} = \int_0^L kAG\left(\sum_{j=1}^{\mu_2}\phi'_{2i}\phi'_{2j}q_{2j} - \sum_{j=1}^{\mu_3}\phi'_{2i}\phi_{3j}q_{3j}\right)\mathrm{d}x \tag{9}$$

$$\frac{\partial U}{\partial q_{3i}} = \int_0^L \left[EI\left(\sum_{j=1}^{\mu_3}\phi'_{3i}\phi'_{3j}q_{3j}\right) + kAG\left(\sum_{j=1}^{\mu_3}\phi_{3i}\phi_{3j}q_{3j} - \sum_{j=1}^{\mu_2}\phi_{3i}\phi'_{2j}q_{2j}\right)\right]\mathrm{d}x \tag{10}$$

2.3 The kinetic energy of the system

The velocity vector $\mathbf{v}$ of an arbitrary point Q (not necessary on the beam axis) in the beam (see Fig. 1) is expressed as

$$\mathbf{v} = \frac{\mathrm{d}\mathbf{r}}{\mathrm{d}t} + \Omega\mathbf{k}\times\mathbf{r} \tag{11}$$

where Ω is the angular speed of the rotating hub, and $\mathbf{r}$ is the vector from the center of the hub to point Q. Using the coordinate system fixed to the rigid hub, $\mathbf{r}$ can be expressed as follows:

$$\mathbf{r} = (r + x + u - z\theta)\mathbf{i} + y\mathbf{j} + (z + w)\mathbf{k} \tag{12}$$

where r is the radius of the rigid hub.

Substituting Eq. (12) into Eq. (11) and noting that both unit vectors $\mathbf{i}$ and $\mathbf{j}$ are time dependent, one can derive the velocity at the arbitrary point Q as follows

$$\mathbf{v} = (\dot{u} - z\dot{\theta} - \Omega y)\mathbf{i} + \Omega(r + x + u - z\theta)\mathbf{j} + \dot{w}\mathbf{k} \tag{13}$$

With the velocity expression (13), the kinetic energy of the rotating beam can be calculated as

$$T = \frac{1}{2}\int_V \rho\mathbf{v}\cdot\mathbf{v}\mathrm{d}V = \frac{1}{2}\int_0^L \rho\int_A \mathbf{v}\cdot\mathbf{v}\mathrm{d}A\mathrm{d}x$$

$$= \frac{1}{2}\int_0^L \rho\left[A\dot{u}^2 + I\dot{\theta}^2 + \Omega^2A(r + x + u)^2 + I\Omega^2\theta^2 + A\dot{w}^2\right]\mathrm{d}x \tag{14}$$

Using Eq. (1) into the kinetic energy expression (14), one obtains the following kinetic energy in terms of the hybrid deformation variables, s, w, and θ

$$T = \frac{1}{2}\int_0^L \rho \left\{ I\dot{\theta}^2 + A\left(\dot{s} - \int_0^x w'\dot{w}'\mathrm{d}\sigma\right)^2 + \Omega^2 A\left[r + x + s - \frac{1}{2}\int_0^x \left(w'\right)^2 \mathrm{d}\sigma\right]^2 + I\Omega^2\theta^2 + A\dot{w}^2 \right\} \mathrm{d}x \tag{15}$$

Substituting Eqs. (2)–(4) into Eq. (15), one obtains the following kinetic energy expression in terms of the generalized coordinates, q_{ij}

$$\begin{aligned} T = \frac{1}{2}\int_0^L \rho \Bigg\{ & I\left(\sum_{j=1}^{\mu_3}\phi_{3j}\dot{q}_{3j}\right)^2 + A\left(\sum_{j=1}^{\mu_1}\phi_{1j}\dot{q}_{1j} - \int_0^x \sum_{j=1}^{\mu_1}\phi'_{1j}q_{1j}\sum_{j=1}^{\mu_1}\phi'_{1j}\dot{q}_{1j}d\sigma\right)^2 \\ & + A\Omega^2\left[r + x + \sum_{j=1}^{\mu_1}\phi_{1j}q_{1j} - \frac{1}{2}\int_0^x\left(\sum_{j=1}^{\mu_2}\phi'_{2j}q_{2j}\right)^2 d\sigma\right]^2 \\ & + I\Omega^2\left(\sum_{j=1}^{\mu_3}\phi_{3j}q_{3j}\right)^2 + A\left(\sum_{j=1}^{\mu_2}\phi_{2j}\dot{q}_{2j}\right)^2 \Bigg\} \mathrm{d}x \end{aligned} \tag{16}$$

To derive the equations of motion, the partial derivatives of T with respect to the generalized coordinates q_{ij} and generalized velocities $\dot{q}_{ij}$ are needed. The derivatives of $\dfrac{\partial T}{\partial \dot{q}_{ij}}$'s with respect to t are also needed. Taking derivatives of T with respect to q_{ij} and $\dot{q}_{ij}$, and neglecting higher order non-linear terms, one has

$$\frac{\partial T}{\partial q_{1i}} = \int_0^L \rho A\Omega^2\left[(r+x)\phi_{1i} + \sum_{j=1}^{\mu_1}\phi_{1i}\phi_{1j}q_{1j}\right]\mathrm{d}x \tag{17}$$

$$\begin{aligned} \frac{\partial T}{\partial q_{2i}} &= -\int_0^L \rho A\Omega^2\left[(r+x)\left(\int_0^x\sum_{j=1}^{\mu_2}\phi'_{2i}\phi'_{2j}q_{2j}d\sigma\right)\right]\mathrm{d}x \\ &= -\int_0^L \rho A\Omega^2[r(L-x) + \frac{1}{2}(L^2 - x^2)]\sum_{j=1}^{\mu_2}\phi'_{2i}\phi'_{2j}q_{2j}\mathrm{d}x \end{aligned} \tag{18}$$

$$\frac{\partial T}{\partial q_{3i}} = \int_0^L \rho\Omega^2 I\sum_{j=1}^{\mu_3}\phi_{3i}\phi_{3j}q_{3j}\mathrm{d}x \tag{19}$$

$$\frac{d}{\mathrm{d}t}\frac{\partial T}{\partial \dot{q}_{1i}} = \int_0^L \rho A\phi_{1i}\left(\sum_{j=1}^{\mu_1}\phi_{1j}\ddot{q}_{1j} - \Omega\sum_{j=1}^{\mu_2}\phi_{2j}\dot{q}_{2j}\right)\mathrm{d}x \tag{20}$$

$$\frac{d}{\mathrm{d}t}\left(\frac{\partial T}{\partial \dot{q}_{2i}}\right) = \int_0^L \rho A\sum_{j=1}^{\mu_2}\phi_{2i}\phi_{2j}\ddot{q}_{2j}\mathrm{d}x \tag{21}$$

$$\frac{d}{\mathrm{d}t}\left(\frac{\partial T}{\partial \dot{q}_{3i}}\right) = \int_0^L \rho I\sum_{j=1}^{\mu_3}\phi_{3i}\phi_{3j}\ddot{q}_{3j}\mathrm{d}x \tag{22}$$

In obtaining Eq. (18), the following relations derived from integration by parts have been used,

$$\int_0^L \left(\rho A \Omega^2 r \int_0^x \sum_{j=1}^{\mu_2} \phi'_{2i} \phi'_{2j} q_{2j} \mathrm{d}\sigma \right) \mathrm{d}x = \int_0^L \rho A \Omega^2 [r(L-x)] \sum_{j=1}^{\mu_2} \phi'_{2i} \phi'_{2j} q_{2j} \mathrm{d}x \tag{23}$$

$$\int_0^L \left(\rho A \Omega^2 x \int_0^x \sum_{j=1}^{\mu_2} \phi'_{2i} \phi'_{2j} q_{2j} \mathrm{d}\sigma \right) \mathrm{d}x = \int_0^L \rho A \Omega^2 \left[\frac{1}{2} \left(L^2 - x^2 \right) \right] \sum_{j=1}^{\mu_2} \phi'_{2i} \phi'_{2j} q_{2j} \mathrm{d}x \tag{24}$$

2.4 Equations of motion

The Lagrange's equations of motion for free vibration of a distributed parameter system is given by [47]

$$\frac{d}{\mathrm{d}t} \left(\frac{\partial T}{\partial \dot{q}_i} \right) - \frac{\partial T}{\partial q_i} + \frac{\partial U}{\partial q_i} = 0 \qquad i = 1, 2, \ldots, \mu \tag{25}$$

where μ is the total number of modal coordinates, and T and U the kinetic energy and potential energy of the beam, respectively.

Substituting Eqs. (8)–(10) and (17)–(22) into Eq. (25), one obtains the following linearized equations of motion

$$\sum_{j=1}^{\mu_1} M_{ij}^{11} \ddot{q}_{1j} + \sum_{j=1}^{\mu_1} \left(K_{ij}^{S} - \Omega^2 M_{ij}^{11} \right) q_{1j} = r \Omega^2 P_{1i} + \Omega^2 Q_{1i}, \qquad i = 1, 2, \ldots, \mu_1 \tag{26}$$

$$\sum_{j=1}^{\mu_2} M_{ij}^{22} \ddot{q}_{2j} + \sum_{j=1}^{\mu_2} \left(K_{ij}^{B2} + \Omega^2 M_{ij}^{\rho 2} \right) q_{2j} - \sum_{j=1}^{\mu_3} K_{ij}^{C23} q_{3j} = 0, \qquad i = 1, 2, \ldots, \mu_2 \tag{27}$$

$$\sum_{j=1}^{\mu_3} M_{ij}^{I3} \ddot{q}_{3j} + \sum_{j=1}^{\mu_3} \left(K_{ij}^{I3} + K_{ij}^{A3} - \Omega^2 M_{ij}^{I3} \right) q_{3j} - \sum_{j=1}^{\mu_2} K_{ij}^{D32} q_{2j} = 0, \qquad i = 1, 2, \ldots, \mu_3 \tag{28}$$

where

$$M_{ij}^{mn} = \int_0^L \rho A \phi_{mi} \phi_{nj} \mathrm{d}x \tag{29}$$

$$M_{ij}^{I3} = \int_0^L \rho I \phi_{3i} \phi_{3j} \mathrm{d}x \tag{30}$$

$$M_{ij}^{\rho n} = \int_0^L \rho A \left[r(L-x) + \frac{1}{2}(L^2 - x^2) \right] \phi'_{ni} \phi'_{nj} \mathrm{d}x \tag{31}$$

$$K_{ij}^{I3} = \int_0^L E I \phi'_{3i} \phi'_{3j} \mathrm{d}x \tag{32}$$

$$K_{ij}^{A3} = \int_0^L k A G \phi_{3i} \phi_{3j} \mathrm{d}x \tag{33}$$

$$K_{ij}^{B2} = \int_0^L kAG\phi'_{2i}\phi'_{2j}\mathrm{d}x \tag{34}$$

$$K_{ij}^{C23} = \int_0^L kAG\phi'_{2i}\phi_{3j}\mathrm{d}x \tag{35}$$

$$K_{ij}^{D32} = \int_0^L kAG\phi_{3i}\phi'_{2j}\mathrm{d}x \tag{36}$$

$$K_{ij}^{S} = \int_0^L EA\phi'_{1i}\phi'_{1j}\mathrm{d}x \tag{37}$$

$$P_{1i} = \int_0^L \rho A\phi_{1i}\mathrm{d}x \tag{38}$$

$$Q_{1i} = \int_0^L \rho Ax\phi_{1i} \tag{39}$$

It is seen that the equation of motion for stretch is not coupled with the equations of motion for flapwise transverse motion.

2.5 Dimensionless transformation

Since the equation of motion for stretch [Eq. (26)] is not coupled with the equations of motion for flapwise transverse motion [Eqs. (27)–(28)]. We will only solve the equations of motion for flapwise transverse motion.

In the present study, the following tapering relations for the height and width of the beam are used.

$$b(x) = b_0\left(1 - c_b\frac{x}{L}\right)^p \tag{40}$$

$$h(x) = h_0\left(1 - c_h\frac{x}{L}\right)^q \tag{41}$$

where b_0 and h_0 are the width and height at the root of the beam, respectively, p and q are the constants depending on the type of taper of the beam, and c_b and c_h are the width and height taper ratios, respectively, defined by

$$c_\mathrm{b} = 1 - \frac{b}{b_0} \tag{42}$$

$$c_\mathrm{h} = 1 - \frac{h}{h_0} \tag{43}$$

In this study, both $p = 1$ and $q = 1$ are used to model a beam that tapers linearly in two planes.

With Eqs. (40) and (41), the variations of the cross-sectional properties can be obtained as

$$A(x) = A_0\left(1 - c_b\frac{x}{L}\right)^p\left(1 - c_h\frac{x}{L}\right)^q \tag{44}$$

$$I(x) = I_0\left(1 - c_b\frac{x}{L}\right)^p\left(1 - c_h\frac{x}{L}\right)^{3q} \tag{45}$$

where A_0 and I_0 are area and the principal moment of inertia about the y-axis at the root cross-section of the beam, respectively.

With the above tapering relations, we can rewrite the equations of motion in a dimensionless form. For this transformation, several dimensionless variables and parameters are defined as follows [44]:

$$\tau = \frac{t}{T} \tag{46}$$

$$\xi = \frac{x}{L} \tag{47}$$

$$\theta_{ij} = \frac{q_{ij}}{L} \tag{48}$$

$$\gamma = \Omega T \tag{49}$$

$$\delta = \frac{r}{L} \tag{50}$$

where T is a generalized time parameter defined as

$$T = \sqrt{\frac{\rho A_0 L^4}{E I_0}} \tag{51}$$

The variables γ and δ represent the angular speed ratio and the hub radius ratio, respectively.

Substituting the dimensionless variables and parameters defined in Eqs. (46)–(51) into Eqs. (27)–(28), the dimensionless equations of motion can be written as

$$\sum_{j=1}^{\mu_2} \overline{M}_{ij}^{22} \ddot{\theta}_{2j} + \sum_{j=1}^{\mu_2} \left(\eta\beta^2 \overline{K}_{ij}^{B2} + \gamma^2 \overline{M}_{ij}^{\rho 2} \right) \theta_{2j} - \eta\beta^2 \sum_{j=1}^{\mu_3} \overline{K}_{ij}^{C23} \theta_{3j} = 0, \quad i = 1, 2, \ldots, \mu_2 \tag{52}$$

$$\sum_{j=1}^{\mu_3} \overline{M}_{ij}^{I3} \ddot{\theta}_{3j} - \eta\beta^4 \sum_{j=1}^{\mu_2} \overline{K}_{ij}^{D32} \theta_{2j} + \sum_{j=1}^{\mu_3} \left(\beta^2 \overline{K}_{ij}^{I3} + \eta\beta^4 \overline{K}_{ij}^{A3} - \gamma^2 \overline{M}_{ij}^{I3} \right) \theta_{3j} = 0, \quad i = 1, 2, \ldots, \mu_3 \tag{53}$$

where

$$\beta = \sqrt{\frac{A_0 L^2}{I_0}} \tag{54}$$

$$\eta = \frac{kG}{E} \tag{55}$$

$$\overline{M}_{ij}^{22} = \int_0^1 (1 - c_b\xi)^p (1 - c_h\xi)^q \psi_{2i} \psi_{2j} \mathrm{d}\xi \tag{56}$$

$$\overline{M}_{ij}^{I3} = \int_0^1 (1 - c_b\xi)^p (1 - c_h\xi)^{3q} \psi_{3i} \psi_{3j} \mathrm{d}\xi \tag{57}$$

$$\overline{M}_{ij}^{\rho 2} = \int_0^1 (1 - c_b\xi)^p (1 - c_h\xi)^q \left[\delta(1 - \xi) + \frac{1}{2}(1 - \xi^2) \right] \psi'_{2i} \psi'_{2j} \mathrm{d}\xi \tag{58}$$

$$\overline{K}_{ij}^{I3} = \int_0^1 (1 - c_b\xi)^p (1 - c_h\xi)^{3q} \psi'_{3i} \psi'_{3j} \mathrm{d}\xi \tag{59}$$

$$\overline{K}_{ij}^{An3} = \int_0^1 (1 - c_b\xi)^p (1 - c_h\xi)^q \psi_{3i} \psi_{3j} \mathrm{d}\xi \tag{60}$$

$$\overline{K}_{ij}^{B2} = \int_0^1 (1 - c_b\xi)^p (1 - c_h\xi)^q \psi'_{2i} \psi'_{2j} \mathrm{d}\xi \tag{61}$$

$$\overline{K}_{ij}^{C23} = \int_0^1 (1 - c_b\xi)^p (1 - c_h\xi)^q \psi'_{2i} \psi_{3j} \mathrm{d}\xi \tag{62}$$

$$\overline{K}_{ij}^{D32} = \int_0^1 (1 - c_b\xi)^p (1 - c_h\xi)^q \psi_{3i} \psi'_{2j} \mathrm{d}\xi \tag{63}$$

in which ψ_{ij} are the normalized assumed modal functions of ξ, and $(\,)'$ denotes the derivative with respect to ξ.

The parameter β is the slenderness ratio of the Timoshenko beam, and η is the effective shear-to-tensile stiffness ratio.

To compute the natural frequencies and their corresponding mode shapes using MATLAB, the equations of motion (52, 53) will be written into a matrix form as follows

$$\mathbf{M}\ddot{\boldsymbol{\theta}} + \mathbf{K}\boldsymbol{\theta} = \mathbf{0} \tag{64}$$

where

$$\mathbf{M} = \begin{bmatrix} \mathbf{M}^{22} & \mathbf{0} \\ \mathbf{0} & \mathbf{M}^{33} \end{bmatrix} \tag{65}$$

$$\mathbf{K} = \begin{bmatrix} \mathbf{K}^{22} & \mathbf{K}^{23} \\ \mathbf{K}^{32} & \mathbf{K}^{33} \end{bmatrix} \tag{66}$$

$$\boldsymbol{\theta} = \begin{Bmatrix} \boldsymbol{\theta}_2 \\ \boldsymbol{\theta}_3 \end{Bmatrix} \tag{67}$$

where the elements of the sub-matrices are defined as

$$M_{ij}^{22} = \overline{M}_{ij}^{22} \tag{68}$$

$$M_{ij}^{33} = \overline{M}_{ij}^{I3} \tag{69}$$

$$K_{ij}^{22} = \eta\beta^2 \overline{K}_{ij}^{B2} + \gamma^2 \overline{M}_{ij}^{\rho 2} \tag{70}$$

$$K_{ij}^{23} = -\eta\beta^2 \overline{K}_{ij}^{C23} \tag{71}$$

$$K_{ij}^{32} = -\eta\beta^4 \overline{K}_{ij}^{D32} \tag{72}$$

$$K_{ij}^{33} = \beta^2 \overline{K}_{ij}^{I3} + \eta\beta^4 \overline{K}_{ij}^{A3} - \gamma^2 \overline{M}_{ij}^{I3} \tag{73}$$

The eigenvalue problem represented by Eq. (64) can be solved by assuming a harmonic motion for $\boldsymbol{\theta}$, i.e.,

$$\boldsymbol{\theta} = \mathrm{e}^{j\omega\tau}\boldsymbol{\Theta} \tag{74}$$

in which j is a imaginary number, ω is the dimensionless natural frequency, and $\boldsymbol{\Theta}$ is the eigenvector (mode shape) corresponding to ω. The actual natural frequency, ω_{beam} of the Timoshenko beam can be calculated from the dimensionless natural frequencies, as

$$\omega_{\text{beam}} = \sqrt{\frac{EI_0}{\rho A_0 L^4}}\,\omega = \sqrt{\frac{E}{\rho}}\frac{\omega}{\beta L} \tag{75}$$

Using Eq. (74) in Eq. (64), we can solve ω from the following eigenvalue problem,

$$\omega^2\mathbf{M}\boldsymbol{\Theta} = \mathbf{K}\boldsymbol{\Theta} \tag{76}$$

where

$$\boldsymbol{\Theta} = \begin{Bmatrix} \boldsymbol{\Theta}^2 \\ \boldsymbol{\Theta}^3 \end{Bmatrix} \tag{77}$$

is the eigenvectors which can be used to calculate the mode shapes for the corresponding natural frequency.

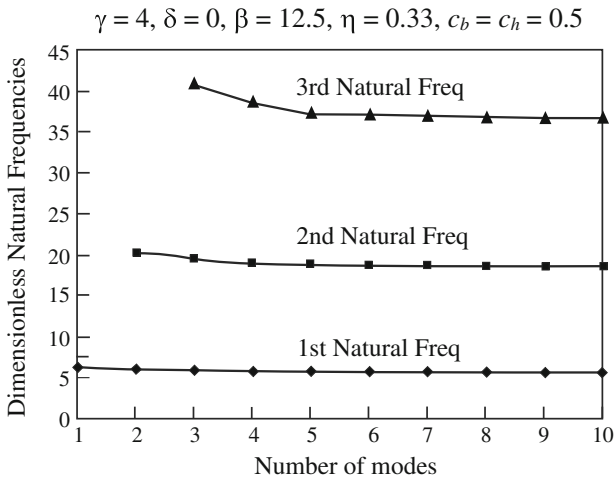

Fig. 2 Convergence of the first three natural frequencies

3 Numerical results

In order to obtain numerical results, several assumed modal functions have been tested to construct the matrices defined in Eqs. (64)–(73). Theoretically, any compact set of functions which satisfy the essential boundary conditions of the Timoshenko beam can be used as the test functions. The normalized modes of a non-rotating Euler–Bernoulli cantilever beam, the orthogonal Legendre polynomials, the polynomial comparison functions, etc., have been tested in the present simulation. All these functions can provide a reasonably accurate result with fewer than 10 assumed modes. The following sections present the results using the normalized modes and their derivatives of a non-rotating Euler–Bernoulli cantilever beam as the modal functions in the simulation.

3.1 Convergence of natural frequencies

The convergence of the first three natural frequencies of a rotating Timoshenko beam is shown in Fig. 2 for a typical set of parameters used in the computation. The "number of modes" in the figure represents the number of the assumed modes for each individual deformation variable. It can be seen from the figure that the natural frequencies converge rapidly as more modes are added in the computation, and using ten modes for each individual deformation variable is sufficient to obtain a reasonable accuracy for the first three natural frequencies. More assumed modes may be required for the higher natural frequencies.

3.2 Comparison of the computational results

To verify the accuracy of the present modeling method, the numerical results from the present modeling method are compared with those presented in Ref. [41]. In Table 1, variation of the natural frequencies of a uniform beam is compared with the ones given in [41] for different slenderness ratios and different angular speeds. It is seen that the natural frequencies increase with an increasing rotational speed and an increasing slenderness ratio. The results obtained from the present method show a maximum of 0.1% difference from those presented in [41].

In Table 2, the natural frequencies of a double-tapered non-rotating Timoshenko beam are compared with those from [41]. The results obtained from the present method show a maximum of 0.11% difference from those presented in [41].

3.3 Effect of the hub radius ratio and rotational speed on the natural frequencies

The variation of the first three natural frequencies of a rotating double-tapered Timoshenko beam with respect to the rotational speed γ and the hub radius ratio δ is shown in Fig. 3. The slenderness ratio $\beta = 30$ and the material parameter $\eta = 0.33$ are used in the simulation. Three hub radius ratios ($\delta = 0,\ 0.5,\ 2$) are considered

Table 1 Comparison of the first four natural frequencies of a non-tapered rotating Timoshenko beam ($\delta = 0$, $\eta = 0.25$)

β	$\gamma = 0$		$\gamma = 4$		$\gamma = 8$		$\gamma = 12$	
	Present	Ref. [41]	Present	Ref. [41]	Present	Ref. [41]	Present	Ref. [41]
Euler–Bernoulli	3.5059	3.5160	5.5850	5.5850	9.2568	9.2568	13.1704	13.1702
	22.0296	22.0345	24.2726	24.2733	29.9950	29.9954	37.6037	37.6031
	61.8502	61.6971	63.9627	63.9666	70.2896	70.2929	79.6136	79.6144
	120.2983	120.9010	123.2354	123.2610	130.0251	130.0490	140.5155	140.5340
50	3.5000	3.4998	5.5623	5.5616	9.2132	9.2096	13.0972	13.0870
	21.3692	21.3547	23.6240	23.6061	29.3501	29.3215	36.9140	36.8659
	57.5636	57.4705	59.9130	59.8117	66.4010	66.2748	75.8382	75.6698
	107.2812	106.9260	109.8286	09.4590	117.0778	116.6650	128.0863	127.6040
25	3.4534	3.4527	5.4980	5.4951	9.0975	9.0854	12.9229	12.8934
	19.6965	19.6497	22.0126	21.9557	27.7933	27.7082	35.3077	35.1811
	49.1256	48.8891	51.7372	51.4822	58.7562	58.4507	68.6107	68.2339
	84.8053	84.1133	87.9002	87.1836	96.4247	95.6423	108.7570	107.8870
16.67	3.3803	3.3787	5.4013	5.3954	8.9423	8.9209	12.7180	12.6724
	17.6251	17.5470	20.0593	19.9662	25.9651	25.8362	33.4388	33.2672
	41.0522	40.7447	44.0648	43.7365	51.7950	51.4154	62.0432	61.6011
	67.0789	66.3623	70.8683	70.1298	80.7277	79.9414	93.8868	93.0672
12.5	3.2863	3.2837	5.2840	5.2749	8.7746	8.7456	12.5134	12.4581
	15.5873	15.4883	18.1781	18.0628	24.1961	24.0479	31.4634	31.2846
	34.6138	34.3005	38.0639	37.7317	46.3420	45.9683	56.3909	55.9744
	54.2503	53.6516	58.5494	57.9491	68.3629	67.8215	77.4992	77.1047
10	3.1774	3.1738	5.1570	5.1448	8.6077	8.5735	12.3066	12.2467
	13.7694	13.6607	16.5184	16.3946	22.4979	22.3506	29.0691	28.9100
	29.6487	29.3614	33.4810	33.1793	41.7829	41.4632	49.9746	49.6484
	44.3234	43.9102	48.1460	47.8101	53.5041	53.2833	56.9137	56.6750

Table 2 Comparison of the first four natural frequencies of a tapered non-rotating Timoshenko beam ($\gamma = 0$, $\beta = 12.50$, $\delta = 0$, $\eta = 0.327$)

c_h	$c_b = 0.0$		$c_b = 0.2$		$c_b = 0.4$		$c_b = 0.6$		$c_b = 0.8$	
	Present	Ref. [41]	Present	Ref. [41]	Present	Ref. [41]	Present	Ref. [41]	Present	Ref. [41]
0.0	3.3273	3.3240	3.5520	3.5485	3.8544	3.8505	4.2926	4.2883	5.0112	5.0062
	16.3052	16.2889	16.6728	16.6561	17.1441	17.1270	17.8047	17.7869	18.9213	18.9024
	36.7440	36.7073	37.0239	36.9869	37.3982	37.3608	37.9595	37.9216	39.0239	38.9849
	58.3361	58.2778	58.5866	58.5281	58.9366	58.8777	59.4920	59.4326	60.6072	60.5467
0.2	3.4314	3.4246	3.6577	3.6504	3.9623	3.9544	4.4041	4.3953	5.1301	5.1199
	15.9223	15.8905	16.2687	16.2362	16.7150	16.6816	17.3456	17.3110	18.4285	18.3917
	35.5010	35.4301	35.7768	35.7054	36.1425	36.0704	36.6873	36.6141	37.7207	37.6454
	57.0048	56.8910	57.2436	57.1293	57.5701	57.4552	58.0789	57.9630	59.0993	58.9813
0.4	3.5712	3.5605	3.7993	3.7879	4.1064	4.0941	4.5522	4.5386	5.2861	5.2703
	15.3989	15.3528	15.7239	15.6769	16.1453	16.0970	16.7462	16.6961	17.7955	17.7423
	33.8890	33.7876	34.1624	34.0602	34.5222	34.4189	35.0543	34.9495	36.0621	35.9542
	54.9204	54.7561	55.1543	54.9893	55.4683	55.3024	55.9488	55.7815	56.9073	56.7371
0.6	3.7698	3.7623	3.9999	3.9919	4.3097	4.3011	4.7593	4.7498	5.4997	5.4887
	14.6741	14.6448	14.9771	14.9472	15.3725	15.3418	15.9424	15.9106	16.9561	16.9223
	31.6871	31.6239	31.9583	31.8945	32.3131	32.2486	32.8343	32.7688	33.8184	33.7509
	51.7257	51.6225	51.9603	51.8566	52.2703	52.1660	52.7362	52.6309	53.6544	53.5473
0.8	4.1259	4.1177	4.3603	4.3516	4.6749	4.6655	5.1296	5.1194	5.8746	5.8629
	13.7849	13.7574	14.0651	14.0370	14.4343	14.4055	14.9738	14.9439	15.9547	15.9229
	28.6933	28.6360	28.9609	28.9031	29.3104	29.2519	29.822	29.7625	30.787	30.7255
	46.9225	46.8288	47.1624	47.0683	47.4759	47.3811	47.9388	47.8431	48.8367	48.7392

in the calculation. As expected, the natural frequencies increase with the increasing rotational speed due to the stiffening effect of the centrifugal force that is directly proportional to Ω^2. Moreover, since the centrifugal force that is directly proportional to the hub radius makes the beam stiffer with the increasing hub radius ratio, the slope of frequency loci increases as the hub radius ratio increases.

3.4 Effect of slenderness ratio

The effect of the slenderness ratio (β) on the natural frequencies is shown in Fig. 4. The ratios of the natural frequencies of a Timoshenko beam over the natural frequencies of an Euler–Bernoulli beam are depicted in the

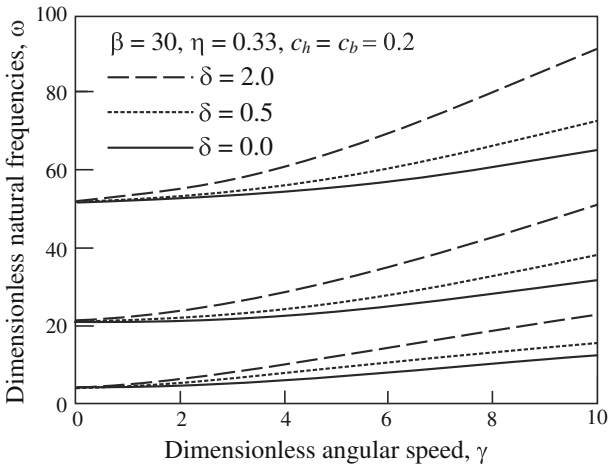

Fig. 3 The first three frequencies for different hub radius ratios

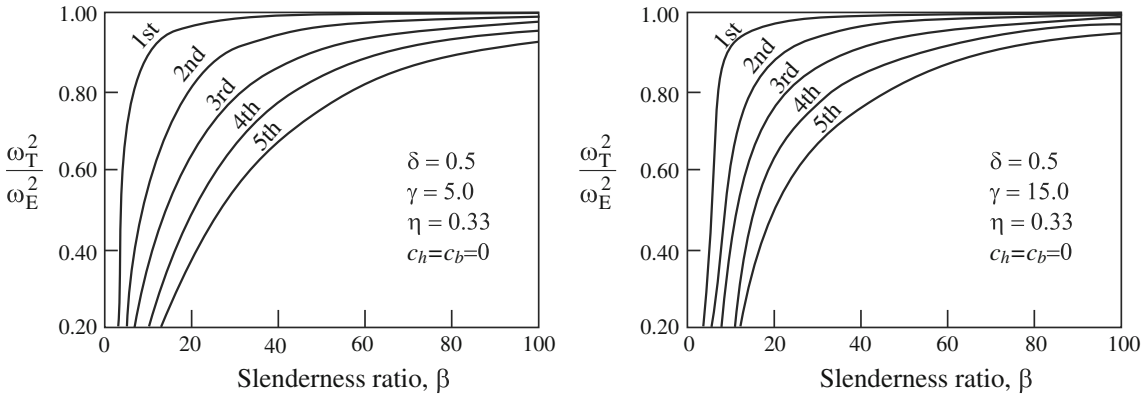

Fig. 4 The effect of the slenderness ratio on the natural frequencies

figure for the first five frequencies. It is seen that the dimensionless natural frequencies increase as the slenderness ratio increases. Please note that the actual natural frequencies of the beam decrease as the slenderness ratio increases and the natural frequencies of a Timoshenko beam are always lower than the natural frequencies of an Euler–Bernoulli beam. It is also seen that the effect of the slenderness ration on the natural frequencies is more significant for a higher rotational speed. Moreover, it is noticed that the effect of the slenderness ratio is dominant on the higher modes and this effect diminishes rapidly as the frequency order decreases. This is something expected because the Timoshenko beam theory is generally used when the higher mode frequencies are of interest.

3.5 Effect of taper ratios

The variation of the natural frequencies of a non-rotating Timoshenko beam with respect to the height taper ratio is shown in Fig. 5. The ratios of the natural frequencies of a tapered beam over the natural frequencies of a non-tapered beam are depicted in the figure for the first three frequencies. It is seen that the height taper ratio has a increasing effect on the first natural frequency, while it has a decreasing effect on the other natural frequencies.

The effect of the width taper ratio on the natural frequencies of a non-rotating Timoshenko beam is shown in Fig. 6. Once again, the ratios of the natural frequencies of a tapered beam over the natural frequencies of a non-tapered beam are depicted in the figure for the first three frequencies. It is seen that the effect of the width taper ratio on the natural frequencies is different from that of the height taper ratio. The width taper ratio has a increasing effect on all natural frequencies. Moreover, the increasing effect is more significant on the fundamental frequency than on the other frequencies.

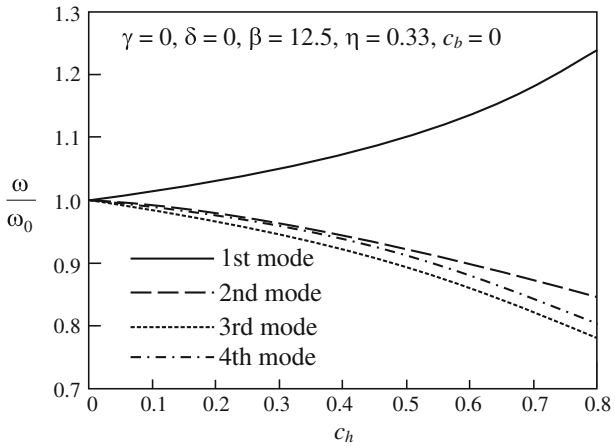

Fig. 5 The effect of the height taper ratio on the natural frequencies

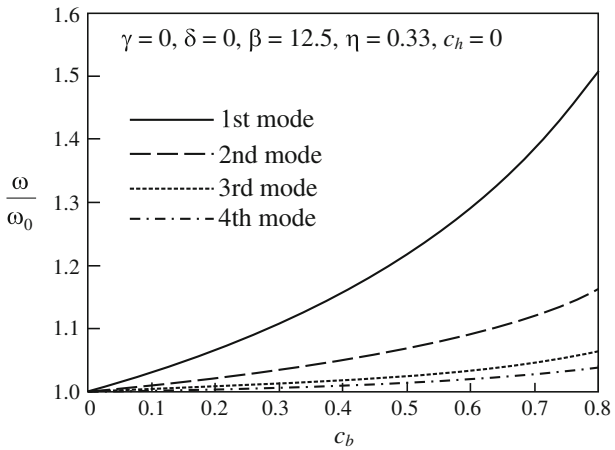

Fig. 6 The effect of the width taper ratio on the natural frequencies

Since both the height and width taper ratios have in increase effect on the first natural frequency, it can be concluded that the first natural frequency of a tapered beam is always higher than that of a non-tapered beam. However, the combined effect of the height and width taper ratios on the higher modes depends on the combination of these two taper ratios. Figure 7 shows the combined effect of the height and width taper ratios on all natural frequencies when $c_h = c_b = 0.5$. It is clear that the combined effect of the height and width taper ratios is significant on the first natural frequency.

3.6 Resonance and tuned angular speed

Resonance will occur when the angular speed of the rotating beam equals to the natural frequency of the beam. The angular speed which causes the resonance is usually called the tuned angular speed [11].

Reference [11] proved that the flapwise tuned angular speed does not exist for a rotating beam from the Euler–Bernoulli theory. However, the tuned angular speed may exist for a rotating Timoshenko beam since the natural frequencies of a Timoshenko beam are lower than the natural frequencies of a Euler–Bernoulli beam. Figure 8 shows the loci of the first two natural frequencies (for $\delta = 0$, $\delta = 1$, and $\delta = 5$) of a non-tapered Timoshenko beam and the straight line of $\omega = \gamma$. The tuned angular speed occurs when the loci of the natural frequencies intersect with the straight line of $\omega = \gamma$. It can be seen that the tuned angular speed occurs at $\gamma = 21.01$ for $\delta = 0$, but it does not exist for $\delta = 1$ and $\delta = 5$.

Since the first natural frequency of a tapered beam is higher than a non-tapered beam, and the tuned angular speed only occurs at the first natural frequency, the taper ratios of the beam have a significant effect on the

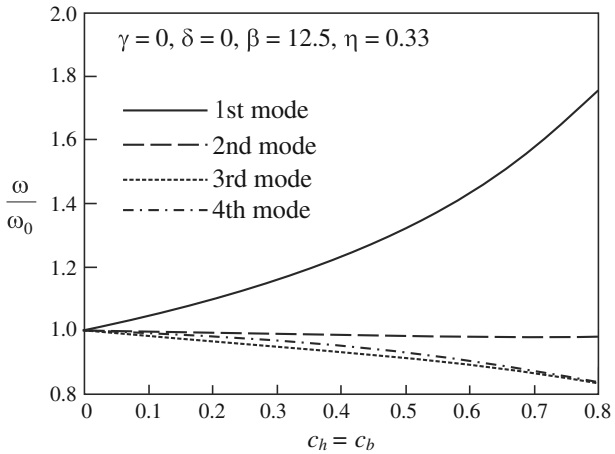

Fig. 7 The combined effect of the height and width taper ratios on the natural frequencies

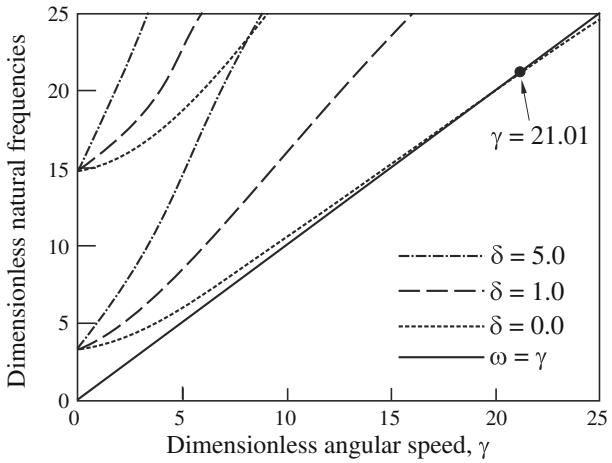

Fig. 8 The tuned angular speed for a non-tapered beam

existence and magnitude of the tuned angular speed of a rotating Timoshenko beam. In our calculation, the tuned angular speed is not found for $c_{\mathrm{h}} = c_{\mathrm{b}} = 0.5$. It may exist mathematically, at a very large angular speed, which is of no practical meaning in engineering applications.

3.7 Mode shape variations

The differences of the first three mode shapes obtained from the Euler–Bernoulli and Timoshenko beam theories are shown in Fig. 9 for a non-tapered beam with $\beta = 10$. Noticeable difference has been observed for the mode shapes with and without considering the shear and rotary effect of the beam.

4 Conclusions

In the present study, the equations of motion for the flapwise vibration analysis of a double-tapered rotating Timoshenko beam are derived using the hybrid deformation variables. The equations of motion are transformed into dimensionless forms in which the dimensionless parameters are identified. The effects of different dimensionless parameters on the natural frequencies are numerically studied. The following results are obtained:

– The natural frequencies increase with the increasing rotational speed due to the stiffening effect of the centrifugal force induced from the rotation. Moreover, this effect is more significant on higher modes than on lower modes.

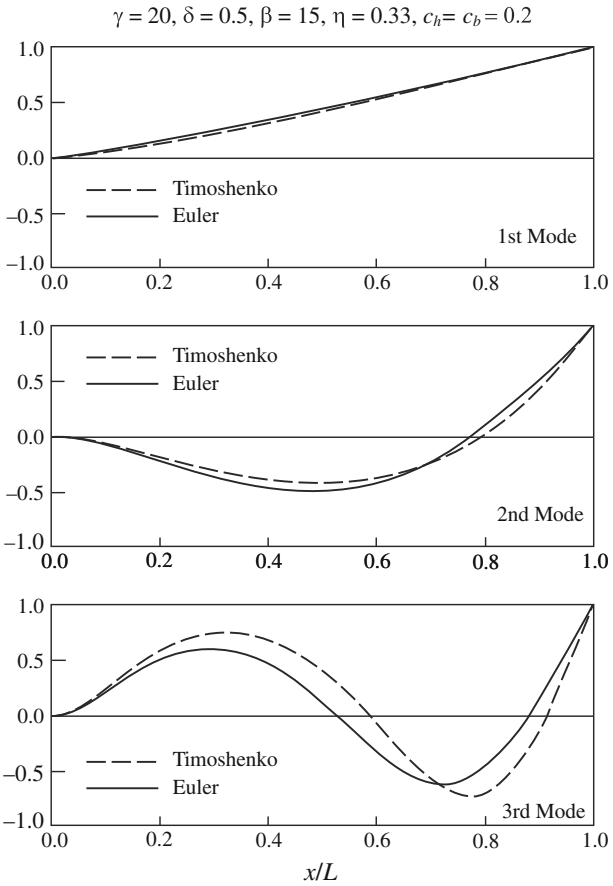

Fig. 9 Mode shape variation due to shear and rotary inertia effect

- The rate of increase in the natural frequencies increases as the hub radius ratio increases.
- Even though the dimensionless natural frequencies increase with an increasing slenderness ratio of a beam, the actual natural frequencies of a rotating Timoshenko bean decrease with an increasing slenderness ratio of the beam. The natural frequencies of a Timoshenko beam are lower than the those of an Euler–Bernoulli beam.
- While the width taper ratio has an increasing effect on all natural frequencies, the height taper ratio has an increasing effect only on the first natural frequency.
- Even though the tuned angular speed was not found from the Euler–Bernoulli beam theory, it may exist in a rotating Timoshenko beam. The existence and magnitude of the tuned angular speed depend on the combination of the height and width taper ratios.

References

1. Southwell, R., Gough, F.: The free transverse vibration of airscrew blades. British A.R.C Reports and Memoranda o.766 (1921)
2. Liebers, F.: Contribution to the theory of propeller vibration. NACA TM No. 568 (1930)
3. Theodorsen, T.: Propeller vibrations and the effect of centrigual force. NACA TN No. 516 (1950)
4. Schilhansl, M.: Bending frequency of rotating cantilever beam. J. Appl. Mech. Trans. Am. Soc. Mech. Eng. **25**, 28–30 (1958)
5. Putter, S., Manor, H.: Natural frequencies of radial rotating beams. J. Sound. Vib. **56**, 175–185 (1978)
6. Hoa, J.: Vibration of a rotating beam with tip mass. J. Sound. Vib. **67**, 369–381 (1979)
7. Bhat, R.: Transverse vibrations of a rotating uniform cantilever beam with tip mass as predicted by using beam characteristic orthogonal polynomials in the Rayleigh–Ritz method. J. Sound. Vib. **105**, 199–210 (1986)
8. Fox, C., Burdress, J.: The natural frequencies of a thin rotating cantilever with offset root. J. Sound. Vib. **65**, 151–158 (1979)
9. Yokoyama, T.: Free vibration characteristics of rotating Timoshenko beams. Int. J. Mech. Sci. **30**, 743–755 (1988)
10. Lee, S., Lin, S.: Bending vibrations of rotating nonuniform Timoshenko beams with an elastically restrained root. J. Appl. Mech. **61**, 949–955 (1994)

11. Yoo, H.H., Shin, S.H.: Vibration analysis of rotating cantilever beams. J. Sound. Vib. **212**, 807–828 (1998)
12. Frisch, H.: A vector-dynamic development of the equations of motion for N-coupled flexible bodies and point masses. NASA TN D-8047 (1975)
13. Ho, J.: Direct path method for flexible multibody spacecraft dynamics. J. Spacecr. Rockets **14**, 102–110 (1977)
14. Hodges, D.H., Dowell, E.H.: Nonlinear equations of motion for the elastic bending and torsion of twisted nonuniform rotor blades. NASA TN D-7818 (1974)
15. Klein, L.: Transverse vibrations of non-uniform beam. J. Sound Vib. **37**, 491–505 (1974)
16. Downs, B.: Transverse vibrations of cantilever beam having unequal breadth and depth tapers. ASMEJ. Appl. Mech. **44**, 737–742 (1977)
17. Swaminathan, M., Rao, J.S.: Vibrations of rotating, pretwisted and tapered blades. Mech. Mach. Theory **12**, 331–337 (1977)
18. Gupta, R.S., Rao, J.S.: Finite element eigenvalue analysis of tapered and twisted Timoshenko beams. J Sound Vib. **56**(2), 187–200 (1978)
19. Hodges, D.: Vibration and response of nonuniform rotating beams with discontinuities. J. Am. Helicopter Soc. **24**, 43–50 (1979)
20. Sato, K.: Transverse vibrations of linearly tapered beams with ends restrained elastically against rotation subjected to axial force. Int. J. Mech. Sci. **22**, 109–115 (1980)
21. Subrahmanyama, K.B., Rao, J.S.: Coupled bending–bending vibrations of pretwisted tapered cantilever beams treated by the Reissner method. Int. J. Eng. Ind. **82**, 577–592 (1982)
22. Lau, J.H.: Vibration frequencies of tapered bars with end mass. ASME J. Appl. Mech. **51**, 179–181 (1984)
23. Banerjee, J.R., Williams, F.W.: Exact Bernoulli–Euler dynamic stiffness matrix for a range of tapered beams. Int. J. Numer. Methods Eng. **21**, 2289–2302 (1985)
24. Banerjee, J.R.: Dynamic stiffness formulation and free vibration analysis of centrifugally stiffened Timoshenko beams. J. Sound Vib. **247**(1), 97–115 (2001)
25. Banerjee, J.R.: Development of an exact dynamic stiffness matrix for free vibration analysis of a twisted Timoshenko beam. J. Sound Vib. **270**, 379–401 (2004)
26. Grossi, R.O., Bhat, R.B.: A note on vibrating tapered beams. J. Sound Vib. **147**, 174–178 (1991)
27. Grossi, R.O., Aranda, A., Bhat, R.B.: Vibration of tapered beams with one end spring hinged and the other end with tip mass. J. Sound Vib. **160**(1), 175–178 (1993)
28. Grossi, R.O., Del, B., Arenas, V.: A variational approach to the vibration of tapered beams with elastically restrained ends. J. Sound Vib. **195**(3), 507–511 (1996)
29. Bazoune, A., Khulief, Y.A.: A finite beam element for vibration analysis of rotating tapered Timoshenko beams. J. Sound Vib. **156**, 141–164 (1992)
30. Khulief, Y.A., Bazoune, A.: Frequencies of rotating tapered Timoshenko beams with different boundary conditions. Comput. Struct. **42**, 781–795 (1992)
31. Naguleswaran, S.: Vibration of an Euler–Bernoulli beam of constant depth and with linearly varying breadth. J. Sound Vib. **153**(3), 509–522 (1992)
32. Naguleswaran, S.: Vibration in the two principal planes of a non-uniform beam of rectangular cross-section, one side of which varies as the square root of the axial co-ordinate. J. Sound Vib. **172**, 305–319 (1994)
33. Naguleswaran, S.: A direct solution for the transverse vibration of Euler–Bernoulli wedge and cone beams. J. Sound Vib. **172**(3), 289–304 (1994)
34. Lee, S.Y., Kuo, Y.H.: Exact solution for the analysis of general elastically restrained non-uniform beams. ASME J. Appl. Mech. **59**, 205–212 (1992)
35. Lee, S.Y., Lin, S.M.: Bending vibrations of a rotating non-uniform beam with an elastically restrained root. J. Sound Vib. **154**(3), 441–451 (1992)
36. Lee, S.Y., Lin, S.M.: Bending vibrations of rotating non-uniform Timoshenko beams with an elastically restrained root. J. Appl. Mech. **61**, 949–955 (1994)
37. Lin, S.M., Wu, C.T., Lee, S.Y.: Analysis of rotating nonuniform pretwisted beams with an elastically restrained root and a tip mass. Int. J. Mech. Sci. **45**, 741–755 (2003)
38. Kaya, M.O.: Free vibration analysis of rotating Timoshenko beams by differential transform method. Aircr. Eng. Aerosp. Tech. **78**(3), 194–203 (2006)
39. Ozdemir Ozgumus, O., Kaya, M.O.: Flexural vibration analysis of double tapered rotating Euler–Bernoulli beam by using the differential transform method. Meccanica **41**(6), 661–670 (2006)
40. Ozdemir, O., Kaya, M.O.: Flapwise bending vibration analysis of a rotating tapered cantilevered Bernoulli–Euler beam by differential transform method. J. Sound Vib. **289**, 413–420 (2006)
41. Ozdemir Ozgumus, O., Kaya, M.O.: Flapwise bending vibration analysis of a rotating double-tapered Timoshenko beam. Arch. Appl. Mech. **78**, 379–392 (2008)
42. Kane, T., Ryan, R., Banerjee, A.: Dynamics of a cantilever beam attached to a moving base. J. Guid. Control Dyn. **10**, 139–151 (1987)
43. Yoo, H., Ryan, R., Scott, R.: Dynamics of flexible beam undergoing overall motions. J. Sound. Vib. **181**, 261–278 (1995)
44. Yoo, H.H., Park, J.H., Park, J.: Vibration analysis of rotating pre-twisted blades. Comput. Struct. **79**, 1811–1819 (2001)
45. Eisenhart, L.: An Introduction to Differential Geometry. Princeton University Press, Princeton (1947)
46. Timoshenko, S.: Vibration Problems in Engineering, 5th edn. Wiley, New York (1990)
47. Craig, R.R.: Structural Dynamics: An Introduction to Computer Methods. Wiley, New York (1981)